

DreamWorld: Unified World Modeling in Video Generation

Boming Tan^{*1} Xiangdong Zhang^{*2} Ning Liao^{*2} Yuqing Zhang¹ Shaofeng Zhang^{†1} Xue Yang² Qi Fan³
Yanyong Zhang¹

Abstract

Despite impressive progress in video generation, existing models remain limited to surface-level plausibility, lacking a coherent and unified understanding of the world. Prior approaches typically incorporate only a single form of world-related knowledge or rely on rigid alignment strategies to introduce additional knowledge. However, aligning the single world knowledge is insufficient to constitute a world model that requires jointly modeling multiple heterogeneous dimensions (e.g., physical commonsense, 3D and temporal consistency). To address this limitation, we introduce **DreamWorld**, a unified framework that integrates complementary world knowledge into video generators via a **Joint World Modeling Paradigm**, jointly predicting video pixels and features from foundation models to capture temporal dynamics, spatial geometry, and semantic consistency. However, naively optimizing these heterogeneous objectives can lead to visual instability and temporal flickering. To mitigate this issue, we propose *Consistent Constraint Annealing (CCA)* to progressively regulate world-level constraints during training, and *Multi-Source Inner-Guidance* to enforce learned world priors at inference. Extensive evaluations show that DreamWorld improves world consistency, outperforming Wan2.1 by 2.26 points on VBench. Code will be made publicly available at [Github](#).

1. Introduction

The landscape of text-to-video (T2V) generation has been transformed by scalable diffusion transformers (Peebles & Xie, 2023; Ma et al., 2025), pushing the field beyond short visual clips toward the ambition of general-purpose world

^{*}Equal contribution ¹University of Science and Technology of China, Hefei, China. ²Shanghai Jiao Tong University, Shanghai, China. ³Nanjing University, Suzhou, China.. Correspondence to: Shaofeng Zhang <sfzhang@ustc.edu.cn>.

Preprint. March 3, 2026.

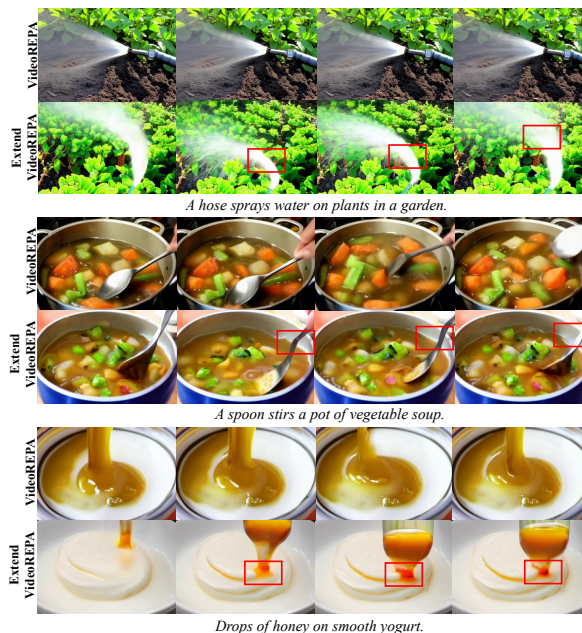


Figure 1. Limitations of extending VideoREPA to multi-source knowledge, leading to structural implausibility and unnatural distortion. The physics score(PC) on the Videophy benchmark dropped from **29.7** to **24.1**.

models (Ha & Schmidhuber, 2018; Brooks et al., 2024). Although state-of-the-art systems such as Lumiere (Bar-Tal et al., 2024), OpenSora (Zheng et al., 2024), and Wan2.1 (Wan et al., 2025) achieve impressive cinematic fidelity through large-scale data and computation, a fundamental gap remains: these models largely function as visual generators rather than world simulators. Optimized primarily for pixel-level distribution matching (Kang et al., 2025; Berg et al., 2025), they fail to internalize structured and comprehensive world knowledge, which is reflected in their limited performance on world-centric benchmarks such as VBench 2.0 (Zheng et al., 2025b).

To mitigate the gap between visual realism and world understanding, prior work (Wu et al., 2025a; Zhang et al., 2025) has explored injecting external world knowledge into video generation models. A representative direction is Representation Alignment (REPA) (Yu et al., 2025b), which aligns generative models with pretrained experts to transfer structured priors. Building on this paradigm, VideoREPA (Zhang

et al., 2025) introduces Token Relation Distillation (TRD) as a soft alignment strategy, demonstrating its effectiveness in distilling knowledge from a single expert model. However, constructing a holistic world model inherently requires the simultaneous integration of *multiple heterogeneous knowledge sources*. Our empirical investigations reveal that naively extending the REPA to concurrently align with semantic, spatial, and dynamic experts leads to a multi-objective optimization dilemma. As illustrated in Figure 1, conflicting relational gradients from distinct teacher models induce optimization instability, suggesting that relational alignment is insufficient for the multi-source integration required by a unified world model (see Appendix A).

In response to these limitations, we propose **DreamWorld**, a unified framework designed to internalize comprehensive world knowledge through a **Joint World Modeling Paradigm**. Inspired by VideoJAM (Chefer et al., 2025), DreamWorld extends standard video latents into a composite feature space, compelling the model to predict video pixels alongside a set of world features. Specifically, DreamWorld integrates temporal dynamics from Optical Flow, spatial geometry from VGGT (Wang et al., 2025a), and semantic understanding from DINOv2 (Oquab et al., 2024).

However, the direct superposition of such heterogeneous optimization objectives frequently induces optimization instability and temporal flickering. To mitigate this, we propose *Consistent Constraint Annealing (CCA)*, a decay mechanism that guarantees convergence by progressively modulating the influence of world knowledge, thereby ensuring high-fidelity visual generation while effectively assimilating world priors. Moreover, a *Multi-Source Inner-Guidance* mechanism is incorporated at inference time, which leverages the model’s own predicted knowledge features to steer the generation process, ensuring trajectories that strictly adhere to real-world laws. **Our main contributions are summarized as follows:**

- i) We present **DreamWorld**, the first unified video generation framework to integrate multi-source world knowledge, including 3D Semantic consistency, Motion Temporal dynamics, and 2D Spatial geometry.
- ii) We propose a novel training strategy, **Consistent Constraint Annealing (CCA)**, which harmonizes knowledge injection with visual quality, ensuring coherent and artifact-free generation.
- iii) Extensive evaluations demonstrate that DreamWorld significantly outperforms baselines and VideoJAM, establishing a new standard for world models.

2. Related Work

Video Diffusion Models. The paradigm of video generation has been revolutionized by the adoption of Diffu-

sion Transformer (DiT) architectures (Peebles & Xie, 2023; Ma et al., 2025) Following the scaling laws originally observed in language modeling (Kaplan et al., 2020) and validated in video (Tong et al., 2025), recent state-of-the-art systems such as Wan2.1 (Wan et al., 2025) and Hunyuan-Video (Kong et al., 2025) have achieved photorealistic results by training on massive video-text corpora. To enhance training stability and inference efficiency beyond standard diffusion, Flow Matching (Lipman et al., 2023) has emerged as a superior generative framework, as successfully implemented in LTX-Video (HaCohen et al., 2026) and Pyramid Flow (Jin et al., 2025). Furthermore, the open-source community has democratized access to high-fidelity generation through open-weights models like Mochi 1 (Team, 2024) and CogVideoX (Yang et al., 2025). Despite these achievements, pure diffusion-based approaches often struggle with real-world understanding, lacking the inherent capability for maintaining global consistency (Qin et al., 2024).

Representation Alignment. Representation Alignment (REPA) (Yu et al., 2025a) addresses the lack of structural awareness in pixel-space diffusion by injecting high-level semantic priors from pre-trained foundation models. Building on this, recent advancements have introduced more sophisticated alignment mechanisms (Zheng et al., 2025a; Jiang et al., 2025; Lee et al., 2025; Li et al., 2025; Zhao et al., 2025). In the video domain, AlignVid (Liu et al., 2025), VideoREPA (Zhang et al., 2025) and MoAlign (Bhowmik et al., 2025) extend this mechanism to spatio-temporal alignment, enforcing adherence to a coherent semantic layout in generated frames. Although these methods offer a pathway to more robust video generation, they typically focus on appearance consistency rather than dynamic causal logic.

World Modeling. The concept of World Models (Ha & Schmidhuber, 2018) transcends video generation, aiming for a rigorous understanding of the environment’s underlying laws to predict and simulate the world. Genie (Bruce et al., 2024) and Genie 2 (Parker-Holder et al., 2024) instantiate this as an interactive simulator, learning a latent action space for controlling video rollouts. Alternatively, the Joint-Embedding Predictive Architecture (JEPA), exemplified by V-JEPA (Bardes et al., 2024) and V-JEPA2 (Assran et al., 2025), utilizes non-generative predictive mechanisms for learning abstract world states. Frame-level (Fuest et al., 2025; Song et al., 2025; Chen et al., 2024; Wu et al., 2025b; Po et al., 2025) context mechanisms introduce frame-level context guidance by adding noise to context frames during training. Additionally, some methods (Xiao et al., 2026) utilize 3D information to enhance spatial coherence. Hybrid approaches such as DriveWorld (Min et al., 2024) and UniWorld (Lin et al., 2025) attempt the unification of generative decoding with state-space modeling. However, existing paradigms lack the capability to synergize knowledge from

multiple heterogeneous expert models (Wu et al., 2025a). Bridging this gap, our work fuses complementary priors, resulting in a world model that surpasses implicit alignment methods in long-horizon consistency and realism.

3. Method

This section outlines the proposed framework. We first introduce the World Knowledge priors and the video diffusion backbone in Section 3.1, followed by the unified preprocessing and alignment protocols in Section 3.2. Section 3.3 then details the Joint World Knowledge Learning (see Fig. 2), optimized via the Consistent Constraint Annealing (CCA) strategy to balance physical constraints and generative fidelity. Finally, Section 3.4 presents the Multi-Source Inner-Guidance mechanism for controllable inference.

3.1. Preliminaries

Video Diffusion Transformers. Recent advances in text-to-video generation, exemplified by models such as Wan2.1 (Wan et al., 2025), utilizes Flow Matching (Lipman et al., 2023) transformers to model the transition from noise to video as a continuous-time process. The pipeline begins with a 3D Causal VAE that compresses the video \mathbf{x} into latent representations $\mathbf{z}_0 = \mathcal{E}(\mathbf{x})$. The core generative mechanism learns to straighten the probability path between the target data \mathbf{z}_0 and the Gaussian prior \mathbf{z}_1 . Defining the intermediate state as:

$$\mathbf{z}_t = t\mathbf{z}_1 + (1-t)\mathbf{z}_0 \quad (1)$$

The model optimizes the velocity field v_θ by regressing against the constant flow $\mathbf{z}_1 - \mathbf{z}_0$:

$$\mathcal{L}_{\text{flow}} = \mathbb{E}_{t, \mathbf{z}_0, \mathbf{z}_1} [\|v_\theta(\mathbf{z}_t, t, \mathbf{c}) - (\mathbf{z}_1 - \mathbf{z}_0)\|^2] \quad (2)$$

where \mathbf{c} represents the conditioning text embeddings. During inference, this learned velocity field guides the generation, allowing the model to recover the video latent $\hat{\mathbf{z}}_0$ by numerically solving the ordinary differential equation (ODE) from $t = 1$ to $t = 0$:

$$\hat{\mathbf{z}}_0 = \mathbf{z}_1 + \int_1^0 v_\theta(\mathbf{z}_\tau, \tau, \mathbf{c}) d\tau \quad (3)$$

WorldKnowledge Priors. We construct a composite feature space, $\mathcal{Z}_{\text{world}}$, that establishes the holistic understanding essential for a world model by unifying three fundamental dimensions of reality. Specifically, *Optical Flow* (Horn & Schunck, 1981) encodes dense pixel-level trajectories for temporal dynamics. *DINOv2* (Oquab et al., 2024) provides robust semantic features to preserve objects following the prompt rules. Finally, *VGGT* (Wang et al., 2025a) explicitly models spatial relationships in 2D geometric constraints.

3.2. Preprocessing

We implement a unified preprocessing protocol comprising motion-to-RGB conversion, spatio-temporal alignment, and

channel compression, thereby aligning heterogeneous priors with the diffusion backbone.

Motion Representation Transformation. Since standard video encoders require RGB inputs, dense displacement fields $\mathbf{d} \in \mathbb{R}^{H \times W \times 2}$ —computed through RAFT (Teed & Deng, 2020)—are mapped into a 3-channel space following the VideoJAM protocol (Chefer et al., 2025).

$$m = \min \left(1, \frac{\sqrt{u^2 + v^2}}{\sigma \sqrt{H^2 + W^2}} \right), \alpha = \arctan2(v, u) \quad (4)$$

where the normalized motion magnitude m and motion direction α are computed from the optical flow components (u, v) to modulate the pixel-wise intensity and hue, respectively, while σ serves as a scaling factor that controls the sensitivity of the motion magnitude normalization. The resulting visualizations are subsequently sampled and encoded by a pre-trained 3D causal VAE (Wan et al., 2025) as videos, yielding the compressed temporal latent $\mathbf{z}_{\text{temporal}}$.

Unified Alignment and Integration. Raw video foundation models (VFM) outputs undergo a dual-alignment process to match the target dimensions. We first resample the spatial dimensions to $H_{\text{lat}} \times W_{\text{lat}}$ by spatial interpolation and then adjust the sequence length by temporal pooling. Recognizing the inherent distributional discrepancy between these heterogeneous expert features and the latent space of the VAE (Higgins et al., 2017), we explicitly apply standardization to harmonize them into a unified statistical manifold. We then employ PCA (Kouzelis et al., 2026) to compress these standardized high-dimensional representations, finally concatenating them along the channel dimension to construct the world latent $\mathbf{Z}_{\text{world}}$:

$$\mathbf{Z}_{\text{world}} = [\mathbf{z}_{\text{temporal}}, \mathbf{z}_{\text{semantic}}, \mathbf{z}_{\text{spatial}}] \quad (5)$$

This compact tensor efficiently conditions the model without introducing excessive computational overhead.

3.3. Joint World Knowledge Learning

Rather than treating $\mathbf{Z}_{\text{world}}$ merely as a conditioning signal (Jang et al., 2025) or directly aligned representation (Yu et al., 2025a), we concatenate $\mathbf{Z}_{\text{world}}$ with the latent and embed the joint features into the diffusion block, enabling the learning of mutual information between visual appearance and underlying world knowledge.

Joint Feature Integration. The core architectural modification in our approach focuses on enabling **joint modeling of video appearance and high-level world knowledge** within a unified transformer framework. Concretely, we expand the linear projection layers to accommodate inputs from both the denoising stream and the world knowledge stream. We extend the pre-trained input projection layer \mathbf{W}_{in} to accommodate the concatenated input

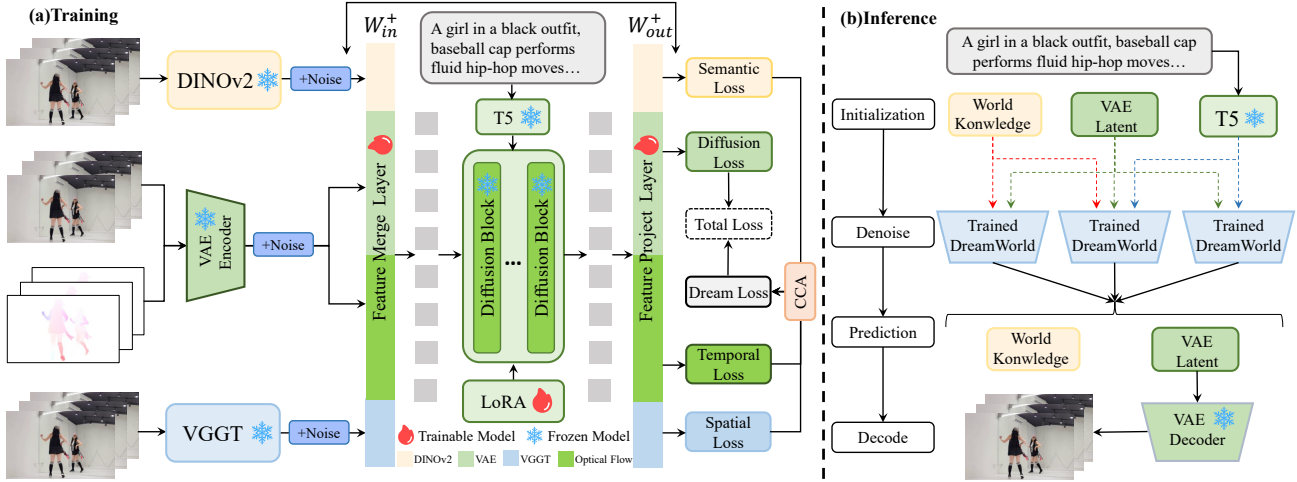


Figure 2. **Overview of DreamWorld.** (a) **Training:** Expert Models are first employed to extract multimodal features, which are then noise-added and concatenated before being fused through a linear layer W_{in}^+ . The resulting prediction is mapped via another linear layer W_{out}^+ to jointly predict appearance and world knowledge, with a Dream Loss constrained by *Consistency Constraint Annealing (CCA)* to ensure generation fidelity. (b) **Inference:** We introduce *Multi-Source Inner-Guidance*, a mechanism that leverages inherent noise features to direct the final video generation process.

$\mathbf{z}_t = [\mathbf{z}_{vae}, \mathbf{Z}_{world}]_t$. The resulting projection layer is defined as:

$$\mathbf{W}_{in}^+ = [\mathbf{W}_{in}, \mathbf{0}] \in \mathbb{R}^{(C_{vae} + C_{world}) \times D} \quad (6)$$

The weights corresponding to \mathbf{Z}_{world} are initialized to **zero**, ensuring that the initial model behavior exactly matches the original pre-trained Wan2.1. This design stabilizes training by preventing abrupt interference from high-dimensional world features, while allowing their influence to be gradually learned through optimization. Symmetrically, the output projection is expanded to $\mathbf{W}_{out}^+ \in \mathbb{R}^{D \times (C_{vae} + C_{world})}$ to predict a joint velocity field, which is subsequently decomposed into modality-specific components:

$$\begin{aligned} \mathbf{z}_{pred} &= \hat{\mathbf{v}}(\mathbf{z}_t, y, t) = \mathbf{M}_{(\mathbf{z}_t \bullet \mathbf{W}_{in}^+)} \bullet \mathbf{W}_{out}^+ \\ &\xrightarrow{\text{split}} [\hat{\mathbf{z}}_{vae}, \hat{\mathbf{z}}_{temporal}, \hat{\mathbf{z}}_{semantic}, \hat{\mathbf{z}}_{spatial}] \end{aligned} \quad (7)$$

where \mathbf{M} denotes the attention blocks and y represents the conditioning prompt.

Training Objective with Consistent Constraint Annealing. The model is optimized using a Flow Matching objective defined over the joint velocity field. The total loss is formulated as a weighted sum of modality-specific flow matching terms:

$$\begin{aligned} \mathcal{L}_{total} &= \mathcal{L}_{vae} + \lambda_{temp}(t) \mathcal{L}_{temporal} \\ &+ \lambda_{sem}(t) \mathcal{L}_{semantic} + \lambda_{spa}(t) \mathcal{L}_{spatial} \end{aligned} \quad (8)$$

Specifically, each individual loss term \mathcal{L}_k , where $k \in \{vae, temporal, semantic, spatial\}$, quantifies the flow matching error between the predicted velocity component

$\hat{\mathbf{z}}_k$ and the target conditional flow $\mathbf{u}_t^{(k)}$ constructed from the ground truth feature \mathbf{z}_k , expressed as the expectation over the time step t , data distribution, and Gaussian noise path:

$$\mathcal{L}_k = \mathbb{E}_{t, \mathbf{z}_k} \left[\left\| \hat{\mathbf{z}}_k(\mathbf{z}_t, y, t) - \mathbf{u}_t^{(k)}(\mathbf{z}_k) \right\|_2^2 \right] \quad (9)$$

where $\mathbf{u}_t^{(k)}$ denotes the target velocity field pointing to the ground truth \mathbf{z}_k . However, a static weighting scheme often exacerbates the inherent tension between maintaining high-fidelity **generative quality** and enforcing effective **knowledge learning** from the introduced features (Fu et al., 2019). To reconcile this conflict, we introduce *Consistent Constraint Annealing (CCA)*. Unlike static strategies, CCA gradually relaxes these weights to zero, prioritizing high-fidelity, artifact-free visual reconstruction in the final phase. Mathematically, the weight $\lambda(t)$ at current training step t is formulated as:

$$\lambda(t) = \lambda_{base} \cdot \frac{1}{2} \left[1 + \cos \left(\pi \frac{t}{T_{total}} \right) \right] \quad (10)$$

where $\lambda_{base} = 0.2$ denotes the initial constraint intensity and T_{total} is the total training duration.

3.4. Multi-Source Inner-Guidance

For precise trajectory correction, we extend standard classifier-free guidance (Vincent, 2011; Ho & Salimans, 2022) to leverage the joint predictions of video latents and physical priors. Formulated within a Bayesian framework, we modify the diffusion score function to independently

Table 1. **Quantitative comparison on VBench.** DreamWorld demonstrates significant improvements over baselines, particularly in temporal dynamics, semantic understanding and spatial relationships, achieving the best performance across all summary scores. **FT** denotes the fine-tuned version, and **Reimpl.** indicates our re-implementation of the method.

Method	Temporal					Semantic				Spatial	Summary		Overall Score	
	Subject Consistency	Background Consistency	Temporal Flickering	Motion Smoothness	Dynamic Degree	Object Class	Color	Human Action	Multiple Objects	Scene	Relationship	Quality Score		Semantic Score
Wan2.1-T2V-1.3B	91.83	94.71	99.17	96.51	65.00	76.09	89.93	74.60	53.66	20.03	62.37	79.81	65.43	76.93
Wan2.1-T2V-1.3B(FT)	93.59	95.81	99.36	97.21	54.08	79.90	88.57	78.98	58.20	28.55	63.31	81.26	68.47	78.71
VideoJAM(Reimpl.)	91.51	96.01	99.13	96.05	73.88	79.22	88.92	79.20	59.66	28.34	66.17	81.18	69.08	78.76
DreamWorld (Ours)	93.62	94.95	98.81	98.07	79.16	81.32	92.61	81.20	65.03	29.71	70.47	83.49	70.89	80.97

Table 2. **Quantitative comparison on VBench-2.0. Abbreviations: Common.:** Commonsense; **Control.:** Controllability; **Hum. Fid.:** Human Fidelity. The best and second-best results are highlighted in **bold** and underlined.

Method	VBench 2.0 Dimensions					Total
	Creativity	Common.	Control.	Hum. Fid.	Physics	
Wan2.1-T2V-1.3B	45.92	59.17	16.81	76.09	55.85	50.77
Wan2.1-T2V-1.3B(FT)	43.13	<u>62.80</u>	18.41	77.09	54.51	51.18
VideoJAM	<u>49.32</u>	64.89	16.33	<u>78.68</u>	52.42	<u>52.33</u>
DreamWorld (Ours)	50.89	61.82	<u>16.95</u>	80.11	<u>55.07</u>	52.97

regulate the influence of each condition k :

$$\nabla \log \tilde{p}_\theta(\mathbf{z}_t|y) \propto \nabla \log p_\theta(\mathbf{z}_t|y) + \sum_{k \in \mathcal{K}} w_k (\nabla \log p_\theta(\mathbf{z}_t|y) - \nabla \log p_\theta(\mathbf{z}_t|y_{-k})) \quad (11)$$

where y_{-k} denotes the condition set with feature $k \in \{text, temporal, semantic, spatial\}$ masked. Adapting this score modification to the Flow Matching velocity domain, the rectified velocity field \mathbf{z}_{pred} is computed as a linear combination of fully conditioned and feature-specific unconditional predictions:

$$\begin{aligned} \mathbf{z}_{pred} \leftarrow & (1 + w_{txt} + w_{temp} + w_{sem} + w_{spa}) \cdot \hat{\mathbf{v}}(\mathbf{z}_t, y, t) \\ & - w_{txt} \cdot \hat{\mathbf{v}}(\mathbf{z}_t, \emptyset, t) \quad (\text{Text Guidance}) \\ & - w_{temp} \cdot \hat{\mathbf{v}}(\mathbf{z}_t^{-temp}, y, t) \quad (\text{Motion Guidance}) \\ & - w_{sem} \cdot \hat{\mathbf{v}}(\mathbf{z}_t^{-sem}, y, t) \quad (\text{Semantic Guidance}) \\ & - w_{spa} \cdot \hat{\mathbf{v}}(\mathbf{z}_t^{-spa}, y, t) \quad (\text{Spatial Guidance}) \end{aligned}$$

where \mathbf{z}_t^{-k} denotes masking the corresponding channel in the World Knowledge tensor. Empirically, we prioritize prompt adherence with $w_{txt} = 5$, while assigning moderate weights $w_{temp} = w_{sem} = w_{spa} = 1$ to the World Knowledge priors.

4. Experiments

4.1. Implementation Details

Model Configuration. The proposed framework is established upon the pre-trained **Wan2.1-T2V-1.3B** (Wan et al., 2025) architecture. The model is configured to synthesize video sequences comprising 81 frames with a spatial resolution of 480×832 . To encapsulate multi-modal world knowledge priors, the joint feature stack employs the pre-trained

Table 3. **Quantitative comparison on VideoPhy benchmark.** We report Semantic Adherence (SA) and Physical Commonsense (PC) scores. The best results are highlighted in **bold**.

Method	Solid-Solid		Solid-Fluid		Fluid-Fluid		Overall	
	SA	PC	SA	PC	SA	PC	SA	PC
Wan2.1-T2V-1.3B	51.1	22.3	45.2	19.1	45.4	23.6	47.7	21.2
Wan2.1-T2V-1.3B(FT)	46.2	18.2	47.8	22.6	50.9	23.6	45.1	20.9
VideoJAM	51.7	29.4	38.4	23.3	47.3	20.1	45.3	25.3
DreamWorld (Ours)	54.5	24.5	48.6	25.4	60.1	32.7	52.9	26.2

RAFT model for optical flow estimation, while semantic and spatial representations are extracted via DINOv2 (Oquab et al., 2024) and VGGT (Wang et al., 2025a), respectively.

Training Details. For training protocol, the WISA (Wang et al., 2025b) open-source dataset is utilized. All video samples are uniformly sampled for 81 frames, and then center-cropped and resized to align with the target resolution of 480×832 . The model was efficiently fine-tuned using LoRA on a subset of 32k WISA videos, with a total of 2,000 optimization steps. The experiments are conducted on a cluster of 8 NVIDIA A100 GPUs with a total batch size of 16. For further elaboration on hyperparameters and architectural specifications, please refer to Appendix B.

4.2. Quantitative Results

For a holistic assessment of generated video quality, the evaluation protocol incorporates the industry-standard VBench and its latest iteration VBench 2.0, VideoPhy, and the unified world generation benchmark, WorldScore.

VBench. The generative capability is systematically evaluated using VBench (Huang et al., 2023), a comprehensive benchmark designed to decompose video generation performance into a hierarchical framework. It evaluates the model from two major dimensions, video quality and semantic consistency, and 16 sub-dimensions, thereby providing a comprehensive assessment of the model’s capabilities as a world model. As detailed in Table 1, DreamWorld demonstrates consistent improvements over both the baseline, Wan2.1-T2V-1.3B (FT), and the competitive VideoJAM method. Specifically, the proposed framework achieves a Total Score

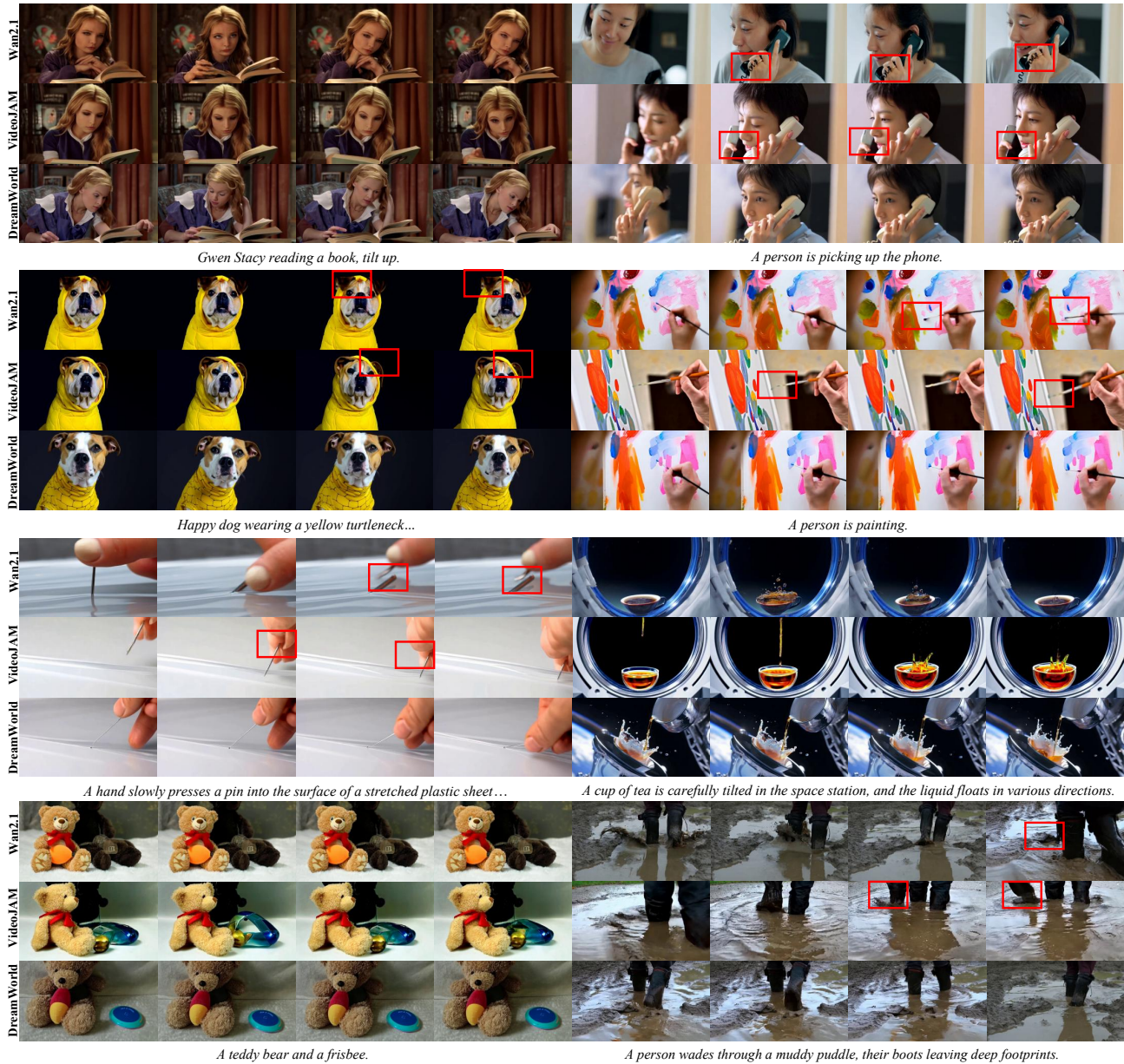


Figure 3. Qualitative comparison of world consistency. DreamWorld outperforms baselines by maintaining semantic realism, spatial integrity, and temporal precision. In contrast, competitor models frequently exhibit geometric penetrations and uncanny distortions

of 80.97, surpassing the baselines by a clear margin. It is observed that the integration of physical priors leads to a marked increase in the Quality Score compared to the fine-tuned baseline, suggesting that physics-aware constraints help refine visual details rather than introducing artifacts. For a more detailed breakdown of performance across all 16 sub-dimensions, please refer to Appendix B.

VBench 2.0. Evaluations are extended to the rigorous VBench 2.0 framework (Zheng et al., 2025b), which employs a refined protocol designed to mirror human perceptual preferences across complex motion and composi-

tional tasks. As quantitative results in Table 2 demonstrate, **DreamWorld** secures the leading position with an aggregate score of **52.97**, outperforming both the large-scale Wan2.1 baselines and the recent VideoJAM. The model proves particularly adept at high-fidelity synthesis highlighting its capability to generate diverse, semantically rich content. Crucially, this aesthetic superiority does not come at the expense of dynamics; our method maintains a highly competitive score, significantly ahead of VideoJAM and Baseline, ultimately striking a superior balance between generative freedom and controllability.

Table 4. Quantitative comparison on WorldScore. Designed to assess the capabilities of world models, this benchmark evaluates simulation logic through static and dynamic scores. The best and second-best results are highlighted in **bold** and underlined.

Method	Static		Dynamic		Overall Score
	3D Consistency	Photometric Consistency	Motion Accuracy	Motion Smoothness	
Wan2.1-T2V-1.3B	72.31	74.41	32.36	68.18	51.03
Wan2.1-T2V-1.3B(FT)	71.73	74.62	35.49	64.76	50.95
VideoJAM	71.53	<u>75.39</u>	33.38	71.95	49.38
DreamWorld (Ours)	73.16	77.55	<u>34.75</u>	<u>69.02</u>	51.48

VideoPhy. We further extend our evaluation to VideoPhy (Bansal et al., 2024), a rigorous benchmark designed to assess physical commonsense in generated videos. Unlike traditional metrics, VideoPhy specifically scrutinizes the model’s ability to adhere to physical laws through Semantic Adherence (SA) and Physical Commonsense (PC), which evaluates compliance with real-world physics. Following WISA (Wang et al., 2025b), when the values of SA and PC are greater than or equal to 0.5, we set them as SA = 1 and PC = 1. Values less than 0.5 are set as SA = 0 and PC = 0.

As presented in Table 3, **DreamWorld** outperforms both the standard Baseline and the motion-prior-based VideoJAM across aggregated metrics. Specifically, our model achieves a state-of-the-art SA of 52.9% and PC of 26.2%, significantly surpassing other leading method. This improvement validates that our world-aware constraints not only enhance the realism of dynamic interactions but also preserve the semantic fidelity of the generation.

WorldScore. We employ **WorldScore** (Duan et al., 2025), a unified benchmark tailored for the rigorous assessment of world simulators, for evaluating the holistic capability of world generation. Diverging from narrow metrics, WorldScore establishes a comprehensive taxonomy that systematically measures performance across **seven static dimensions** and **three dynamic dimensions**. This stratified approach explicitly differentiates between static visual quality and dynamic temporal coherence, providing a macroscopic and objective view of model efficacy.

Results in Table 4 show that DreamWorld demonstrates a consistent lead in aggregated metrics achieving a Total Score of **51.48**, outperforming both the fine-tuned Wan2.1 baseline and VideoJAM. This quantitative evidence confirms that the proposed framework effectively balances static fidelity with dynamic evolution, resulting in a superior overall capacity for realistic world simulation.

4.3. Qualitative Results

We compare DreamWorld against VideoJAM and Wan2.1 to evaluate world modeling capabilities. As illustrated in

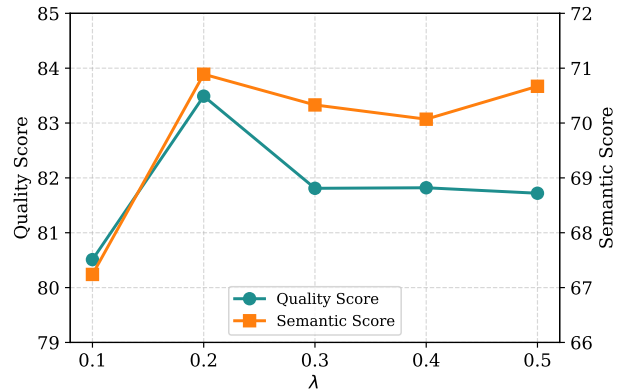


Figure 4. Influence of loss weights λ. Quantitative comparison of generation quality and semantic alignment across different weight settings. The results indicate that λ = 0.2 yields the best trade-off.

Figure 3, our method exhibits superior world consistency. Semantically, in the space station scenario, our model accurately follows the prompt to carefully tilt the cup, allowing the liquid to flow down naturally; in contrast, both VideoJAM and Baseline fail to initiate the critical tilting action. Spatially, the happy dog demonstrates excellent 3D occlusion, ensuring the ears and turtleneck sweater are correctly positioned without physically impossible penetration. Temporally, as seen in the Gwen Stacy reading example, our model generates smooth and natural motion consistent and the character’s facial identity remains stable, avoiding the temporal deformations often observed in baseline methods. These results demonstrate that injecting multi-modal world knowledge effectively constrains the diffusion process, ensuring strict alignment with real-world logic. Please refer to Appendix C for further qualitative comparisons.

4.4. Ablation Studies

The efficacy of DreamWorld is validated through a three-dimensional analysis, with VBench consistently employed as the default benchmark for ablation experiments, barring any specific exceptions.

Effectiveness of World Knowledge The necessity of the comprehensive WorldKnowledge stack is rigorously validated by progressively evaluating its constituent feature subsets. As shown in Table 5, relying on the spatial prior (**VGGT Only**) provides basic geometric grounding but lacks semantic coherence. The integration of the semantic prior (**VGGT + DINOv2**) significantly bolsters the model’s capabilities, particularly in maintaining object permanence and ensuring precise text-video alignment. Nevertheless, the optimal performance is achieved only by the full model, confirming that the synergy of spatial guidance, semantic context, and temporal consistency is essential for robust and realistic world simulation.

Table 5. **Ablation studies on DreamWorld.** We analyze the effectiveness of our method from two perspectives: (1) different **feature integration strategies**, and (2) the **Multi-Source Inner-Guidance** mechanism by selectively removing components. Best results are highlighted in **bold**.

Method	Quality	Semantic	Overall
VGGT Only	81.76	71.36	79.68
VGGT + DINOv2	82.08	71.58	79.98
w/o Text Guidance	77.09	47.41	71.15
w/o VGGT Guidance	81.84	70.87	79.65
w/o DINOv2 Guidance	81.98	70.95	79.78
w/o Optical Flow	81.87	71.06	79.71
DreamWorld (Ours)	83.49	70.89	80.97

Effectiveness of CCA. The qualitative efficacy of Consistent Constraint Annealing (CCA) is evidenced by the visual artifacts observed in the static weighting baseline. Without the dynamic schedule, optimization conflicts manifest as severe abnormal highlighting and exposure anomalies, particularly visible in the Balcony scenes where lighting becomes unnaturally intense. Furthermore, temporal instability is evident in the Grazing Cow and Moving Sheep, which suffers from high-frequency flickering and texture jittering. The proposed CCA strategy effectively eliminates these artifacts, allowing the model to refine visual details without interference, thus ensuring both photorealism and temporal smoothness.

Effectiveness of Multi-Source Inner-Guidance. We investigate the necessity of integrating diverse priors through an ablation study on the Multi-Source Inner-Guidance mechanism (Table 5). The results indicate that removing any individual component leads to consistent performance degradation. Notably, excluding Temporal Priors causes the most significant drop in Quality and Overall scores, the absence of Text Guidance or Semantic Priors severely impairs the Semantic score. Ultimately, DreamWorld achieves superior performance, confirming that the synergistic integration of text, semantic, spatial, and temporal cues is essential for a robust physics-aware world model.

Influence of λ . We investigate the sensitivity of our model to the loss weight λ , which controls the strength of the world knowledge priors. To quantify the trade-off between generative fidelity and condition adherence, we report both the Quality Score and Semantic Score on VBench across varying λ values. As illustrated in Fig. 4, the performance of both metrics peaks at $\lambda = 0.2$. We observe that lower values fail to effectively enforce the physical and semantic constraints, whereas excessive weights interfere with the diffusion backbone’s distribution, leading to a degradation in visual quality. Consequently, we adopt $\lambda = 0.2$ as the

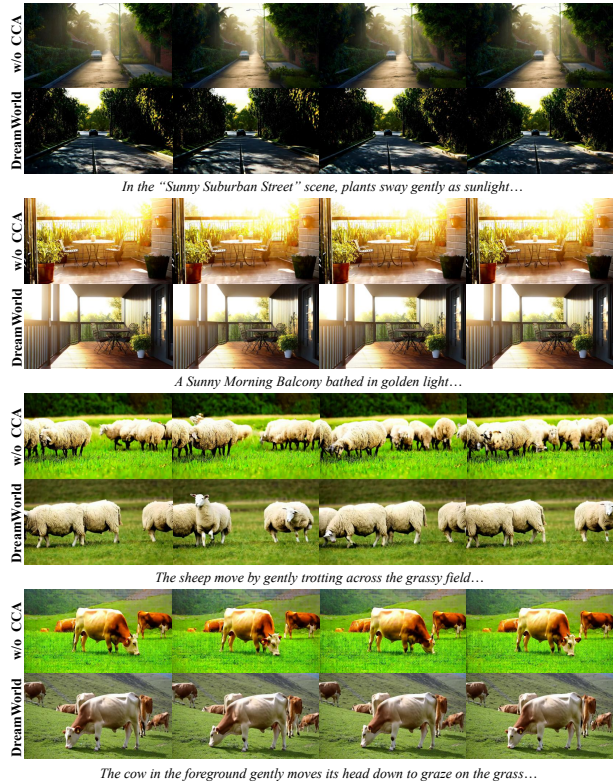


Figure 5. **Effectiveness of CCA.** Without CCA, the generated videos suffer from severe flickering and abnormal highlighting artifacts, leading to degraded visual quality.

optimal configuration for our full model.

5. Conclusion

In this work, we presented **DreamWorld**, a unified framework designed to bridge the prevailing gap between high-fidelity video synthesis and intrinsic world coherence. We identify that previous approaches often focus on distilling a single expert model. However, directly enforcing simultaneous alignment across multiple knowledge sources is prone to collapsing into trivial solutions due to conflicting optimization objectives. We introduced a softer **Joint World Modeling Paradigm** that facilitates the synergistic integration of multi-source expert knowledge. This gentle alignment approach, complemented by our *Consistent Constraint Annealing (CCA)* strategy and *Multi-Source Inner-Guidance*, effectively harmonizes the intricate interplay between structural logic and generative freedom. DreamWorld establishes a new state-of-the-art on standard benchmarks, validating its potential as a robust foundation for next-generation general-purpose world simulators.

Limitations. Despite these advancements, our approach is currently constrained by the computational resources and the diversity of the training datasets. Future research could explore optimizing the efficiency of this multi-source in-

tegration and incorporating more diverse data curation to further enhance the universality of the simulated world.

Impact Statement

This paper aims to advance the development of world models in the field of video generation. While we are fully aware of the recognized ethical challenges and facing generative media, the contributions of this research are essentially within the scope of methodology and fundamental theory. Therefore, this work does not introduce any new specific ethical risks or loopholes beyond those inherent in existing video synthesis techniques. We share the position of the broader academic community in firmly supporting responsible and sustainable technology development to ensure the safety and fairness of generative tools. Ultimately, we are committed to fostering a research environment where technical progress aligns with rigorous ethical standards

References

- Assran, M., Bardes, A., Fan, D., Garrido, Q., Howes, R., Mojtaba, Komeili, Muckley, M., Rizvi, A., Roberts, C., Sinha, K., Zholus, A., Arnaud, S., Gejji, A., Martin, A., Hogan, F. R., Dugas, D., Bojanowski, P., Khalidov, V., Labatut, P., Massa, F., Szafraniec, M., Krishnakumar, K., Li, Y., Ma, X., Chandar, S., Meier, F., LeCun, Y., Rabbat, M., and Ballas, N. V-jepa 2: Self-supervised video models enable understanding, prediction and planning, 2025. URL <https://arxiv.org/abs/2506.09985>.
- Bansal, H., Lin, Z., Xie, T., Zong, Z., Yarom, M., Bitton, Y., Jiang, C., Sun, Y., Chang, K.-W., and Grover, A. Videophy: Evaluating physical commonsense for video generation, 2024. URL <https://arxiv.org/abs/2406.03520>.
- Bar-Tal, O., Chefer, H., Tov, O., Herrmann, C., Paiss, R., Zada, S., Ephrat, A., Hur, J., Liu, G., Raj, A., Li, Y., Rubinstein, M., Michaeli, T., Wang, O., Sun, D., Dekel, T., and Mosseri, I. Lumiere: A space-time diffusion model for video generation, 2024. URL <https://arxiv.org/abs/2401.12945>.
- Bardes, A., Garrido, Q., Ponce, J., Rabbat, M., LeCun, Y., Assran, M., and Ballas, N. Revisiting feature prediction for learning visual representations from video. *arXiv:2404.08471*, 2024.
- Berg, J., Zhu, C., Bao, Y., Durugkar, I., and Gupta, A. Semantic world models, 2025. URL <https://arxiv.org/abs/2510.19818>.
- Bhowmik, A., Korzhenkov, D., Snoek, C. G. M., Habibian, A., and Ghafoorian, M. Moalign: Motion-centric representation alignment for video diffusion models, 2025. URL <https://arxiv.org/abs/2510.19022>.
- Brooks, T., Peebles, B., Holmes, C., DePue, W., Guo, Y., Jing, L., Schnurr, D., Taylor, J., Luhman, T., Luhman, E., Ng, C., Wang, R., and Ramesh, A. Video generation models as world simulators. 2024. URL <https://openai.com/research/video-generation-models-as-world-simulators>.
- Bruce, J., Dennis, M., Edwards, A., Parker-Holder, J., Shi, Y., Hughes, E., Lai, M., Mavalankar, A., Steigerwald, R., Apps, C., Aytar, Y., Bechtle, S., Behbahani, F., Chan, S., Heess, N., Gonzalez, L., Osindero, S., Ozair, S., Reed, S., Zhang, J., Zolna, K., Clune, J., de Freitas, N., Singh, S., and Rocktäschel, T. Genie: Generative interactive environments, 2024. URL <https://arxiv.org/abs/2402.15391>.
- Chefer, H., Singer, U., Zohar, A., Kirstain, Y., Polyak, A., Taigman, Y., Wolf, L., and Sheynin, S. Videojam: Joint appearance-motion representations for enhanced motion generation in video models, 2025. URL <https://arxiv.org/abs/2502.02492>.
- Chen, B., Monso, D. M., Du, Y., Simchowitz, M., Tedrake, R., and Sitzmann, V. Diffusion forcing: Next-token prediction meets full-sequence diffusion, 2024. URL <https://arxiv.org/abs/2407.01392>.
- Duan, H., Yu, H.-X., Chen, S., Fei-Fei, L., and Wu, J. Worldscore: A unified evaluation benchmark for world generation, 2025. URL <https://arxiv.org/abs/2504.00983>.
- Fu, H., Li, C., Liu, X., Gao, J., Celikyilmaz, A., and Carin, L. Cyclical annealing schedule: A simple approach to mitigating kl vanishing, 2019. URL <https://arxiv.org/abs/1903.10145>.
- Fuest, M., Hu, V. T., and Ommer, B. Maskflow: Discrete flows for flexible and efficient long video generation, 2025. URL <https://arxiv.org/abs/2502.11234>.
- Ha, D. and Schmidhuber, J. World models. 2018. doi: 10.5281/ZENODO.1207631. URL <https://zenodo.org/record/1207631>.
- HaCohen, Y., Brazowski, B., Chiprut, N., Bitterman, Y., Kvochko, A., Berkowitz, A., Shalem, D., Lifschitz, D., Moshe, D., Porat, E., Richardson, E., Shiran, G., Chachy, I., Chetboun, J., Finkelson, M., Kupchick, M., Zabari, N., Guetta, N., Kotler, N., Bibi, O., Gordon, O., Panet, P., Benita, R., Armon, S., Kulikov, V., Inger, Y., Shiftan, Y., Melumian, Z., and Farbman, Z. Ltx-2: Efficient joint audio-visual foundation model, 2026. URL <https://arxiv.org/abs/2601.03233>.

- Higgins, I., Matthey, L., Pal, A., Burgess, C., Glorot, X., Botvinick, M., Mohamed, S., and Lerchner, A. beta-vae: Learning basic visual concepts with a constrained variational framework. In *International conference on learning representations*, 2017.
- Ho, J. and Salimans, T. Classifier-free diffusion guidance, 2022. URL <https://arxiv.org/abs/2207.12598>.
- Horn, B. K. and Schunck, B. G. Determining optical flow. *Artificial Intelligence*, 17(1):185–203, 1981. ISSN 0004-3702. doi: [https://doi.org/10.1016/0004-3702\(81\)90024-2](https://doi.org/10.1016/0004-3702(81)90024-2). URL <https://www.sciencedirect.com/science/article/pii/0004370281900242>.
- Huang, Z., He, Y., Yu, J., Zhang, F., Si, C., Jiang, Y., Zhang, Y., Wu, T., Jin, Q., Chanpaisit, N., Wang, Y., Chen, X., Wang, L., Lin, D., Qiao, Y., and Liu, Z. Vbench: Comprehensive benchmark suite for video generative models, 2023. URL <https://arxiv.org/abs/2311.17982>.
- Jang, J., Kim, J., Baek, K., and Kwak, N. Multi-dimensional preference alignment by conditioning reward itself, 2025. URL <https://arxiv.org/abs/2512.10237>.
- Jiang, D., Wang, M., Li, L., Zhang, L., Wang, H., Wei, W., Dai, G., Zhang, Y., and Wang, J. No other representation component is needed: Diffusion transformers can provide representation guidance by themselves, 2025. URL <https://arxiv.org/abs/2505.02831>.
- Jin, Y., Sun, Z., Li, N., Xu, K., Xu, K., Jiang, H., Zhuang, N., Huang, Q., Song, Y., Mu, Y., and Lin, Z. Pyramidal flow matching for efficient video generative modeling, 2025. URL <https://arxiv.org/abs/2410.05954>.
- Kang, B., Yue, Y., Lu, R., Lin, Z., Zhao, Y., Wang, K., Huang, G., and Feng, J. How far is video generation from world model: A physical law perspective, 2025. URL <https://arxiv.org/abs/2411.02385>.
- Kaplan, J., McCandlish, S., Henighan, T., Brown, T. B., Chess, B., Child, R., Gray, S., Radford, A., Wu, J., and Amodei, D. Scaling laws for neural language models, 2020. URL <https://arxiv.org/abs/2001.08361>.
- Kong, W., Tian, Q., Zhang, Z., Min, R., Dai, Z., Zhou, J., Xiong, J., Li, X., Wu, B., Zhang, J., Wu, K., Lin, Q., Yuan, J., Long, Y., Wang, A., Wang, A., Li, C., Huang, D., Yang, F., Tan, H., Wang, H., Song, J., Bai, J., Wu, J., Xue, J., Wang, J., Wang, K., Liu, M., Li, P., Li, S., Wang, W., Yu, W., Deng, X., Li, Y., Chen, Y., Cui, Y., Peng, Y., Yu, Z., He, Z., Xu, Z., Zhou, Z., Xu, Z., Tao, Y., Lu, Q., Liu, S., Zhou, D., Wang, H., Yang, Y., Wang, D., Liu, Y., Jiang, J., and Zhong, C. Hunyuanvideo: A systematic framework for large video generative models, 2025. URL <https://arxiv.org/abs/2412.03603>.
- Kouzelis, T., Karypidis, E., Kakogeorgiou, I., Gidaris, S., and Komodakis, N. Boosting generative image modeling via joint image-feature synthesis, 2026. URL <https://arxiv.org/abs/2504.16064>.
- Langley, P. Crafting papers on machine learning. In Langley, P. (ed.), *Proceedings of the 17th International Conference on Machine Learning (ICML 2000)*, pp. 1207–1216, Stanford, CA, 2000. Morgan Kaufmann.
- Lee, J.-Y., Cha, B., Kim, J., and Ye, J. C. Aligning text to image in diffusion models is easier than you think, 2025. URL <https://arxiv.org/abs/2503.08250>.
- Li, Z., Meng, L., Chao, G., Wu, W., Yan, X., Yang, Y., Qi, Z., and Meng, X. Semantic-space-intervened diffusive alignment for visual classification, 2025. URL <https://arxiv.org/abs/2505.05721>.
- Lin, B., Li, Z., Cheng, X., Niu, Y., Ye, Y., He, X., Yuan, S., Yu, W., Wang, S., Ge, Y., et al. Uniworld: High-resolution semantic encoders for unified visual understanding and generation. *arXiv preprint arXiv:2506.03147*, 2025.
- Lipman, Y., Chen, R. T. Q., Ben-Hamu, H., Nickel, M., and Le, M. Flow matching for generative modeling, 2023. URL <https://arxiv.org/abs/2210.02747>.
- Liu, Y., Shu, W.-J., Huang, Z., Zheng, H., Wang, Y., Zhang, M., Lim, S.-N., and Yang, H. Alignvid: Training-free attention scaling for semantic fidelity in text-guided image-to-video generation, 2025. URL <https://arxiv.org/abs/2512.01334>.
- Ma, X., Wang, Y., Chen, X., Jia, G., Liu, Z., Li, Y.-F., Chen, C., and Qiao, Y. Latte: Latent diffusion transformer for video generation, 2025. URL <https://arxiv.org/abs/2401.03048>.
- Min, C., Zhao, D., Xiao, L., Zhao, J., Xu, X., Zhu, Z., Jin, L., Li, J., Guo, Y., Xing, J., Jing, L., Nie, Y., and Dai, B. Driveworld: 4d pre-trained scene understanding via world models for autonomous driving, 2024. URL <https://arxiv.org/abs/2405.04390>.
- Oquab, M., Darcet, T., Moutakanni, T., Vo, H., Szafraniec, M., Khalidov, V., Fernandez, P., Haziza, D., Massa, F., El-Nouby, A., Assran, M., Ballas, N., Galuba, W., Howes, R., Huang, P.-Y., Li, S.-W., Misra, I., Rabbat, M., Sharma, V., Synnaeve, G., Xu, H., Jegou, H., Mairal, J., Labatut, P., Joulin, A., and Bojanowski, P. DINOv2: Learning robust visual features without supervision, 2024. URL <https://arxiv.org/abs/2304.07193>.

- Parker-Holder, J., Ball, P., Bruce, J., Dasagi, V., Holsheimer, K., Kaplanis, C., Moufarek, A., Scully, G., Shar, J., Shi, J., Spencer, S., Yung, J., Dennis, M., Kenjeyev, S., Long, S., Mnih, V., Chan, H., Gazeau, M., Li, B., Pardo, F., Wang, L., Zhang, L., Besse, F., Harley, T., Mitenkova, A., Wang, J., Clune, J., Hassabis, D., Hadsell, R., Bolton, A., Singh, S., and Rocktäschel, T. Genie 2: A large-scale foundation world model. 2024. URL <https://deepmind.google/discover/blog/genie-2-a-large-scale-foundation-world-model>
- Peebles, W. and Xie, S. Scalable diffusion models with transformers, 2023. URL <https://arxiv.org/abs/2212.09748>.
- Po, R., Nitzan, Y., Zhang, R., Chen, B., Dao, T., Shechtman, E., Wetzstein, G., and Huang, X. Long-context state-space video world models, 2025. URL <https://arxiv.org/abs/2505.20171>.
- Qin, Y., Shi, Z., Yu, J., Wang, X., Zhou, E., Li, L., Yin, Z., Liu, X., Sheng, L., Shao, J., Bai, L., Ouyang, W., and Zhang, R. Worldsimbench: Towards video generation models as world simulators, 2024. URL <https://arxiv.org/abs/2410.18072>.
- Song, K., Chen, B., Simchowitz, M., Du, Y., Tedrake, R., and Sitzmann, V. History-guided video diffusion, 2025. URL <https://arxiv.org/abs/2502.06764>.
- Team, G. Mochi 1. <https://github.com/genmoai/models>, 2024.
- Teed, Z. and Deng, J. Raft: Recurrent all-pairs field transforms for optical flow, 2020. URL <https://arxiv.org/abs/2003.12039>.
- Tong, J., Mou, Y., Li, H., Li, M., Yang, Y., Zhang, M., Chen, Q., Liang, T., Hu, X., Zheng, Y., Chen, X., Zhao, J., Huang, X., and Qiu, X. Thinking with video: Video generation as a promising multimodal reasoning paradigm, 2025. URL <https://arxiv.org/abs/2511.04570>.
- Vincent, P. A connection between score matching and denoising autoencoders. *Neural computation*, 23(7):1661–1674, 2011.
- Wan, T., Wang, A., Ai, B., Wen, B., Mao, C., Xie, C.-W., Chen, D., Yu, F., Zhao, H., Yang, J., Zeng, J., Wang, J., Zhang, J., Zhou, J., Wang, J., Chen, J., Zhu, K., Zhao, K., Yan, K., Huang, L., Feng, M., Zhang, N., Li, P., Wu, P., Chu, R., Feng, R., Zhang, S., Sun, S., Fang, T., Wang, T., Gui, T., Weng, T., Shen, T., Lin, W., Wang, W., Wang, W., Zhou, W., Wang, W., Shen, W., Yu, W., Shi, X., Huang, X., Xu, X., Kou, Y., Lv, Y., Li, Y., Liu, Y., Wang, Y., Zhang, Y., Huang, Y., Li, Y., Wu, Y., Liu, Y., Pan, Y., Zheng, Y., Hong, Y., Shi, Y., Feng, Y., Jiang, Z., Han, Z., Wu, Z.-F., and Liu, Z. Wan: Open and advanced large-scale video generative models, 2025. URL <https://arxiv.org/abs/2503.20314>.
- Wang, J., Chen, M., Karaev, N., Vedaldi, A., Rupprecht, C., and Novotny, D. Vgggt: Visual geometry grounded transformer, 2025a. URL <https://arxiv.org/abs/2503.11651>.
- Wang, J., Ma, A., Cao, K., Zheng, J., Zhang, Z., Feng, J., Liu, S., Ma, Y., Cheng, B., Leng, D., Yin, Y., and Liang, X. Wisa: World simulator assistant for physics-aware text-to-video generation, 2025b. URL <https://arxiv.org/abs/2502.08153>.
- Wu, H., Wu, D., He, T., Guo, J., Ye, Y., Duan, Y., and Bian, J. Geometry forcing: Marrying video diffusion and 3d representation for consistent world modeling, 2025a. URL <https://arxiv.org/abs/2507.07982>.
- Wu, T., Yang, S., Po, R., Xu, Y., Liu, Z., Lin, D., and Wetzstein, G. Video world models with long-term spatial memory, 2025b. URL <https://arxiv.org/abs/2506.05284>.
- Xiao, Z., Lan, Y., Zhou, Y., Ouyang, W., Yang, S., Zeng, Y., and Pan, X. Worldmem: Long-term consistent world simulation with memory, 2026. URL <https://arxiv.org/abs/2504.12369>.
- Yang, Z., Teng, J., Zheng, W., Ding, M., Huang, S., Xu, J., Yang, Y., Hong, W., Zhang, X., Feng, G., Yin, D., Zhang, Y., Wang, W., Cheng, Y., Xu, B., Gu, X., Dong, Y., and Tang, J. Cogvideox: Text-to-video diffusion models with an expert transformer, 2025. URL <https://arxiv.org/abs/2408.06072>.
- Yu, S., Kwak, S., Jang, H., Jeong, J., Huang, J., Shin, J., and Xie, S. Representation alignment for generation: Training diffusion transformers is easier than you think. In *International Conference on Learning Representations*, 2025a.
- Yu, S., Kwak, S., Jang, H., Jeong, J., Huang, J., Shin, J., and Xie, S. Representation alignment for generation: Training diffusion transformers is easier than you think, 2025b. URL <https://arxiv.org/abs/2410.06940>.
- Zhang, X., Liao, J., Zhang, S., Meng, F., Wan, X., Yan, J., and Cheng, Y. Videorepa: Learning physics for video generation through relational alignment with foundation models, 2025. URL <https://arxiv.org/abs/2505.23656>.
- Zhao, P., Luan, R., Zhang, W., Wu, P., and He, S. Guiding cross-modal representations with mllm priors via preference alignment, 2025. URL <https://arxiv.org/abs/2506.06970>.

Zheng, B., Ma, N., Tong, S., and Xie, S. Diffusion transformers with representation autoencoders, 2025a. URL <https://arxiv.org/abs/2510.11690>.

Zheng, D., Huang, Z., Liu, H., Zou, K., He, Y., Zhang, F., Gu, L., Zhang, Y., He, J., Zheng, W.-S., Qiao, Y., and Liu, Z. Vbench-2.0: Advancing video generation benchmark suite for intrinsic faithfulness, 2025b. URL <https://arxiv.org/abs/2503.21755>.

Zheng, Z., Peng, X., Yang, T., Shen, C., Li, S., Liu, H., Zhou, Y., Li, T., and You, Y. Open-sora: Democratizing efficient video production for all, 2024. URL <https://arxiv.org/abs/2412.20404>.

A. Motivation Experiments

Investigating the feasibility of simultaneously assimilating comprehensive physical and semantic knowledge, we implemented an extended experimental scheme labeled **Extend-VideoREPA**, incorporating three independent projection layers—configured with output dimensions of 768, 2048, and 768—to map the VAE latent into the distinct embedding spaces of **DINOv2**, **VGGT**, and **VideoMAEv2**.

By formulating the total training objective as the summation of the standard diffusion loss and the independent Token Relation Distillation (TRD) terms from each expert branch, we compel the generative backbone to concurrently reconstruct the internal relational topology of these diverse feature spaces, thereby internalizing multi-source knowledge through a unified soft alignment paradigm.

B. Implementation Details

Training Configuration. We initialize the generative backbone with the pre-trained weights of Wan2.1, while the newly introduced expanded projection layers are initialized to zero to strictly preserve the initial generative distribution. We employ the AdamW optimizer with hyperparameters $\beta_1 = 0.9$, $\beta_2 = 0.99$, and a weight decay of $\lambda = 0.2$. The learning rate is set to $1e - 5$ with seed 42, utilizing a linear warmup for the first 400 steps followed by a consistency-constrained annealing strategy. To optimize memory efficiency and throughput, we utilize Mixed Precision Training (BF16) alongside gradient checkpointing.

Feature Extraction and Alignment. For the WorldKnowledge priors, we employ state-of-the-art visual foundation models to extract offline features, ensuring high-quality guidance signals. Specifically, dense optical flow fields are first computed using RAFT (Teed & Deng, 2020). Crucially, to align with the generative backbone, these 2D displacement fields are converted into RGB visualizations (as detailed in Section 3.2) and subsequently encoded by the frozen Wan2.1 VAE (Wan et al., 2025). This maps the motion dynamics into the native latent space, resulting in a temporal feature dimension of $C_{temporal} = 16$. For semantic and spatial representations, we utilize the frozen DINOv2 (Oquab et al., 2024) and VGGT (Wang et al., 2025a) encoders. After spatial alignment and temporal pooling, we apply PCA to compress the channel dimensions of these features to $C_{semantic} = 8$ and $C_{spatial} = 8$, respectively. Consequently, the final composite input fed into the expanded projection layer consists of the noisy video latents $C_{vae} = 16$ concatenated with the WorldKnowledge priors, yielding a total input channel dimensionality of $C_{total} = 48$.

Inference Setup. During inference, videos are generated using the Flow Matching Euler Discrete Scheduler with 50 denoising steps. We apply the proposed Multi-Faceted Self-Guidance with a text guidance scale of $w_{text} = 5$ to ensure prompt fidelity. The auxiliary guidance scales for motion, semantics, and geometry are empirically set to $w_{temporal} = w_{semantic} = w_{spatial} = 1$. This configuration was chosen based on ablation studies to provide subtle yet effective structural rectification without introducing high-frequency artifacts.

B.1. Results of WorldScore

Detailed multidimensional metrics for WorldScore are presented in Table B.1 .

Table B.1. Quantitative comparison on WorldScore. The best and second-best results are highlighted in **bold** and underlined.

Method	Static Attributes					Dynamic Attributes			Summary		Overall Score		
	Camera Control	Object Control	Content Alignment	3D Consistency	Photometric Consistency	Style Consistency	Subjective Quality	Motion Accuracy	Motion Magnitude	Motion Smoothness		Static Score	Dynamic Score
Wan2.1-T2V-1.3B	23.50	52.34	66.83	72.31	74.40	34.08	52.21	32.36	34.14	68.18	53.66	44.89	51.03
Wan2.1-T2V-1.3B(FT)	23.66	49.66	<u>65.35</u>	71.73	74.62	39.04	53.83	35.49	31.35	64.76	<u>53.98</u>	43.86	50.95
VideoJAM	22.48	57.34	59.32	71.53	<u>75.39</u>	25.90	44.03	33.38	<u>32.51</u>	71.95	50.86	45.94	49.38
DreamWorld (Ours)	22.81	51.94	64.95	73.16	77.55	<u>35.75</u>	<u>52.45</u>	<u>34.75</u>	32.44	<u>69.02</u>	54.09	<u>45.41</u>	51.48

B.2. VBench and VBench2.0 Results

We report the detailed breakdown of metrics on both VBench and VBench-2.0 benchmarks, providing a granular analysis of model performance. The comprehensive evaluations for VBench are presented in Table B.2 and Table B.3, while the VBench-2.0 results are detailed in Table B.4, Table B.5, and Table B.6.

DreamWorld: Unified World Modeling in Video Generation

Table B.2. Results of VBench (Part 1/2): Consistency, Motion, and Object-level Metrics.

Method	Subject Consistency	Background Consistency	Temporal Flickering	Motion Smoothness	Dynamic Degree	Aesthetic Quality	Imaging Quality	Object Class	Multiple Objects	Human Action
Wan2.1-T2V-1.3B	91.83	94.71	99.17	96.51	65.00	57.24	59.14	76.09	53.66	74.60
Wan2.1-T2V-1.3B(FT)	93.59	95.81	99.36	97.21	54.08	61.13	63.27	79.90	58.20	78.98
VideoJAM	91.51	96.01	99.13	96.05	73.88	58.41	62.68	79.22	59.66	79.20
DreamWorld (Ours)	93.62	94.95	98.81	98.07	79.16	59.59	66.76	81.32	65.03	81.20

Table B.3. Results of VBench (Part 2/2): Appearance, Style, and Overall Scores.

Method	Color	Spatial Relationship	Scene	Appearance Style	Temporal Style	Overall Consist.	Quality Score	Semantic Score	Overall Score
Wan2.1-T2V-1.3B	89.93	62.37	20.03	22.91	22.23	24.25	79.81	65.43	76.93
Wan2.1-T2V-1.3B(FT)	88.57	63.31	28.55	22.38	23.93	24.94	81.26	68.47	78.71
VideoJAM	88.92	66.17	28.34	22.67	24.03	25.01	81.18	69.08	78.76
DreamWorld (Ours)	92.61	70.47	29.71	22.14	23.82	24.87	83.49	70.89	80.97

Table B.4. VBench-2.0 results (part 1/3).

Method	Human Identity	Dynamic Spatial Relationship	Complex Landscape	Instance Preservation	Multi-View Consistency	Human Clothes	Dynamic Attribute	Complex Plot
Wan2.1-T2V-1.3B	64.21	26.57	16.22	80.41	14.63	99.55	22.34	10.53
Wan2.1-T2V-1.3B (FT)	72.43	28.50	21.66	88.24	8.24	90.13	22.71	11.77
VideoJAM	72.14	24.08	15.66	90.41	6.79	97.74	24.37	10.33
DreamWorld (Ours)	71.68	24.15	14.66	86.14	12.41	99.11	26.73	10.44

Table B.5. VBench-2.0 results (part 2/3).

Method	Mechanics	Human Anatomy	Composition	Human Interaction	Motion Rationality	Material	Diversity	Motion Order Understanding
Wan2.1-T2V-1.3B	85.71	64.51	40.19	15.00	37.93	57.77	51.65	7.31
Wan2.1-T2V-1.3B (FT)	88.63	68.71	39.35	14.66	37.35	60.67	46.91	6.42
VideoJAM	80.31	66.51	44.81	17.33	39.37	56.62	53.84	7.53
DreamWorld (Ours)	86.30	69.35	45.01	19.00	38.51	55.17	56.76	8.88

Table B.6. VBench-2.0 results (part 3/3).

Method	Camera Motion	Thermotics	Creativity Score	Commonsense Score	Controllability Score	Human Fidelity Score	Physics Score	Total Score
Wan2.1-T2V-1.3B	19.75	65.27	45.92	59.17	16.81	76.09	55.85	50.77
Wan2.1-T2V-1.3B (FT)	23.14	60.49	43.13	62.80	18.41	77.09	54.51	51.18
VideoJAM	15.04	61.97	49.32	64.89	16.33	78.68	52.42	52.33
DreamWorld (Ours)	14.81	66.43	50.89	61.82	16.95	80.11	55.07	52.97

As evidenced by the quantitative data, **DreamWorld** demonstrates robust superiority over the baselines. In VBench, our method achieves significant margins in Spatial Relationship and Dynamic Degree, which contributes to a leading Overall Score of 80.97. Furthermore, on the more challenging VBench-2.0, DreamWorld secures the highest Total Score (52.97) and excels in complex categories such as Human Fidelity and Motion Order Understanding. These results validate that our joint world modeling paradigm effectively internalizes multi-modal priors, resulting in generated content with real-world fidelity.

C. More qualitative results

We provide additional qualitative comparisons in Figure C.1 to further substantiate the superiority of DreamWorld over the baseline Wan2.1. These visual results underscore our model’s robustness across semantic, spatial, and temporal dimensions. Specifically, in complex interaction scenarios such as eating ice cream or cutting a bell pepper, the baseline frequently succumbs to semantic hallucinations and spatial conflicts, where objects unnaturally fuse or distort. Conversely, DreamWorld maintains clear object boundaries and logical interaction physics.

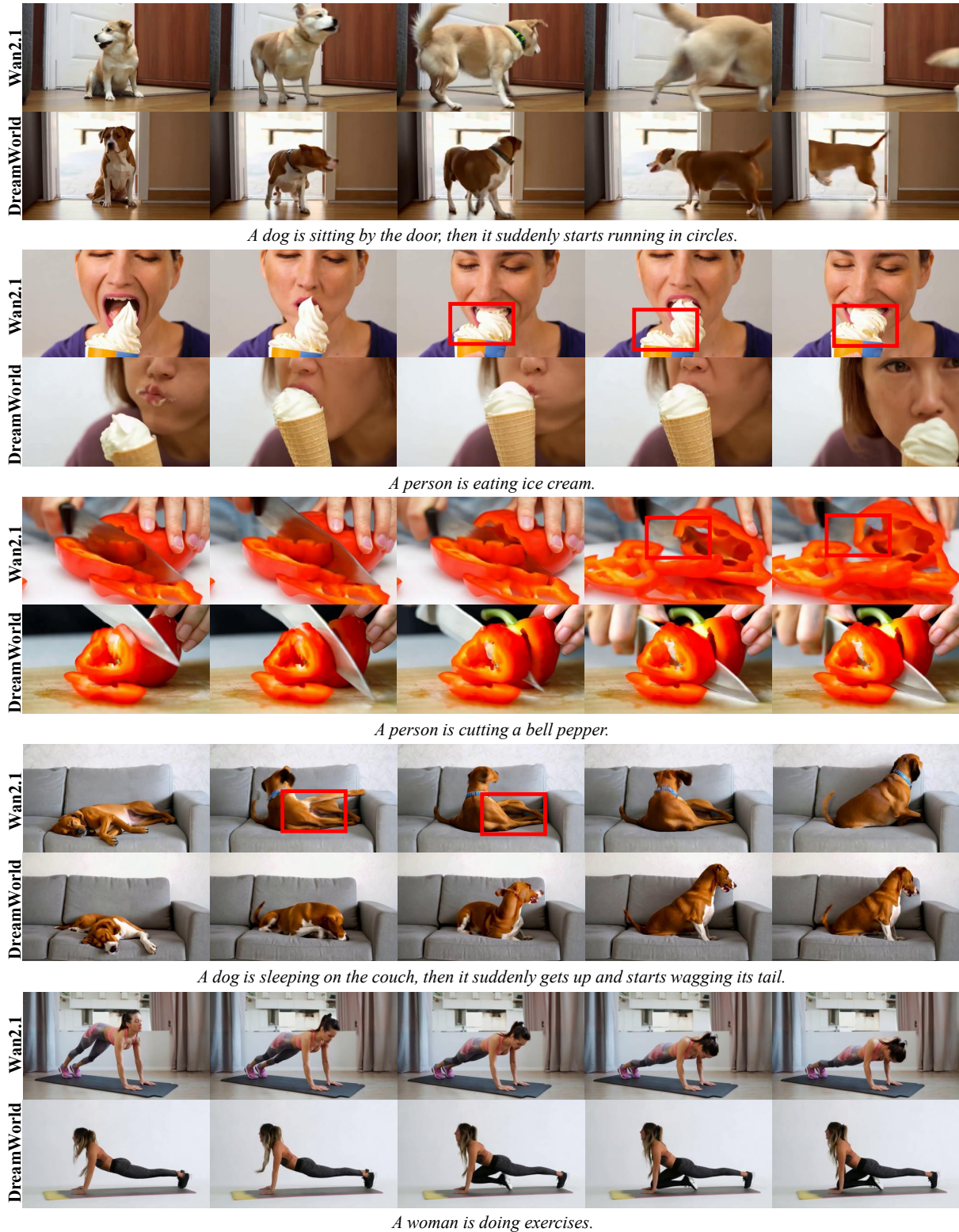


Figure C.1. **Additional qualitative comparisons.** The top rows display results from Wan2.1, while the bottom rows show results from our DreamWorld. The red rectangles highlight anomalies (e.g., object penetration, unnatural disappearance, and limb distortion). In contrast, DreamWorld exhibits superior structural integrity and dynamic coherence across diverse scenarios.